Organic planar diode with Cu electrode via modification of the metal surface by SAM of fluorobiphenyl based thiol

Swarup Biswas[1], Philippe Decorse[2], Hyeok Kim[1]*, Philippe Lang[2]*

[1]*School of Electrical and Computer Engineering, Institute of Information Technology University of Seoul, 163 Seoulsiripdaero, Dongdaemun-gu, Seoul 02504, Republic of Korea.*

[2] *Université de Paris, CNRS, ITODYS, F-75006 Paris, France*

*Corresponding Author

Tel.: 82-2-6490-2354 fax: 82-2-6490-2314. E-mail address: hyeok.kim@uos.ac.kr (H. Kim)

Tel.: +33 (0)157277260 fax: +33 (0)157277263. E-mail address: lang@u-paris.fr (P. Lang)

Abstract

The surface of a Cu electrode is modified by the combination of preliminary oxidative treatment and grafting of a bifunctional self-assembled monolayer based on fluorobiphenylthiol (FBPS) or biphenylthiol (BPS). In these conditions, a dinaphtho [2, 3-b: 2′,3′-f] thieno [3,2-b] thiophene (DNTT)-based diode exhibits high mobility (0.35 $cm^2.V^{-1}.s^{-1}$) due to the formation of organized assembly of FBPS on the oxide copper that has been partially reduced in Cu_2O; this organization controls that of the semiconductor film. On the other hand, the same treatment of Cu electrode with BPS molecules does not function, due to the disorganization of both the BPS SAM and the DNTT film. These results suggest that a monolayer of dipolar-oriented molecules lowers the injection barrier; steers the semiconductor organization and thereby enhances the performance of the derived electronic component.

Keywords: self-assembled monolayers, copper, biphenyl thiol, organic diode, metal-semiconductor interface, contact resistance

1. Introduction

Demand of organic semiconductor-based electronic devices such as organic diodes [1], organic thin-film transistors [2], organic photovoltaic cells [3-4], organic light-emitting diodes [5], etc. is growing day by day. Charge injection from a conducting electrode to a semiconducting active material plays a vital role in the operation of these devices. Gold (Au) is the perfect choice for the electrode material due to its good conductivity, very high chemical stability, and optimal work function [6]. However, the use of expensive Au for electrodes is not suitable for manufacturing low-cost electronic devices. To overcome this limitation, nowadays, more attention is being paid, easily available such as silver (Ag), copper (Cu) and aluminum (Al) [7-8] that would drastically reduce manufacturing costs. The main drawbacks to this approach are the energy barrier due to work function mismatch, between the metallic electrodes and the semiconductor active layer, and the oxidation of the metal and its consequences. To reduce the energy barrier at the interface between the metal electrode and the semiconducting active layer, in 1996, Campbell et al. introduced an efficient technique [9]. They tuned the Schottky energy barriers in organic electronic devices by grafting self-assembled monolayers (SAMs) on the metallic (Ag) electrode surface. Subsequently, many people adopted this technique to improve performance in various applications such as protective coatings, electronic devices, chemical sensors, etc. [10-13]. In 2007, Heimel et al. validated the interpretation of this technique by quantum mechanical simulation [14].

A self-assembled monolayer (SAM) is a two-dimensional assembly of ordered organic molecules that is grafted onto the surface of a substrate by the adsorption of molecules with a specific affinity of their head-groups for the substrate [15]. Usually the thickness of a SAM is between 1 nm and 3 nm. The main advantage of using a SAM is that it can remarkably tune

the surface chemistry of a substrate [16]. Moreover, the dipole formed by the SAM may have both positive and negative effects [13] on the injection of charge in a semiconductor (SC). If the orientation of the dipole favors the appropriate charge transfer mechanism, the energy barrier for the carriers at the metal-SC interface will decrease. On the other hand, if the orientation of the dipole hinders charge transfer at the interface, the energy barrier will increase. Depending on the nature of the SC, holes or electron carriers, the work function (W) of the electrode should increase or decrease to promote the adequate charge transfer, respectively. Therefore, selection or tailoring of molecules for SAM treatment of the electrode is a very important task. For example, recently Kim et al. have observed that hole injection from Au electrode to pentacene can be improved significantly by SAM treatment of Au with the dipolar 4'-fluoro-**1**,**1**'-biphenyl-4-**thiol** (FBPS); in the SAM the fluorine atom is negatively charged and the dipole is directed towards the metal (-→+). On the other hand, hole injection from the Au electrode to pentacene is hindered significantly by SAM treatment of an Au electrode by the unsubstituted **1**,**1**'-biphenyl-4-**thiol** (BPS), whose dipole is in the opposite direction [13]. They have explained the results in terms of the adjustment of the injection barrier height by the interface dipole induced by the self-assembled monolayer. Initially, alkane-based molecules were used as SAMs to modify the surface of the metal electrode in different electronic devices due to their well-ordered 2-D structures but, due to their insulating nature, it was necessary to compromise with the reduction of charge injection ability [17-18 -19]. In this respect, different conjugated molecules with a phenyl moiety, such as thiophenols, perform better [16, 20-21]. Cu is a cheap and highly conductive metal but until now it has not been utilized as electrode material in sophisticated electronic devices due to its lower work function and environmental instability (oxidized in air).

Therefore, in this work we modified the surface of a cheap Cu electrode by the combination of preliminary oxidative RCA treatment and the grafting of a bifunctional SAM such as

FBPS or BPS. A dinaphtho [2, 3-b: 2′,3′-f] thieno [3,2-b] thiophene (DNTT) based diode with a Cu electrode preliminary oxidative treatment and grafting of a bifunctional self-assembled monolayer showed high mobility due to the formation of highly organized FBPS dipoles on its surface. On the other hand, the grafting of BPS on the Cu electrode oxidized as previously did not function well, in particular due to the disorganization of the BPS SAM on the surface of the electrode.

2. Experimental Details

2.1. Materials

BPS and FBPS (Fluorochem) (Fig. 1a) were used without any further treatment. The thiol solvent was dichloromethane (Aldrich, HPLC grade) and was used after treatment by Na_2CO_3 (0.5M in water) and distillation under dinitrogen, stored under argon and protected from light. The solvent was in some cases carefully dried and stored on Al_2O_3 beads previously heated at 300°C for 1h (SD solvent). Ammonia (NH_3) solution (25% in water) and hydrogen peroxide (H_2O_2, 25% in water) were obtained from Aldrich.

Dinaphtho[2,3-b:2′,3′-f]thieno[3,2-b]thiophene (DNTT) was purchased from Aldrich and used as received. Copper was evaporated under vacuum onto glass. Gold films on glass substrates were from Arrandee Metal GmbH + Co. KG.

2.2. Treatment of electrode

To control the reproducibility and stability of the SAM/Cu system, the Cu/glass substrate was oxidized by a NH_3/ H_2O_2/H_2O solution (RCA treatment in the following) in ratio (v/v/v) 1/1/400 to 1/1/32000 RCA for 2 minutes at 80 ^oC. We present here the optimal treatments obtained with ratios of 1/1/:4000 and 1/1/16000. BPS and FBPS solutions (10^{-3} M)

were prepared in CH_2Cl_2 or SD [13]. After the RCA treatment, the Cu substrate was rinsed with ultra-pure water (18MΩ.cm, ELGA), then by CH_2Cl_2 and finally placed in the thiol solution immediately to avoid any contamination. The dipping time was 1h. After that, the Cu substrates were rinsed thoroughly twice with dichloromethane (2x 2min), dried and stored under argon. Au slides were dipped 30 times (2 s each dip) in a water–ethanol 50/50 vol. % mixture in an ultrasonic bath. They were then passed quickly 3–6 times through a hydrogen flame for ca. 0.5 s, cooled under argon, rinsed with water and CH_2Cl_2 and immediately immersed in the thiol solution.

2.3 Determination of orientation of thiol-based SAM deposited on Cu

Previously it has been observed that the orientation of the dipole molecules in a SAM is a very important factor for SAM-treated metal electrodes [13]. It can affect charge carrier injection from the electrode to the semiconductor layer. SAMs are generally oriented at an angle (α) with respect to the normal (Fig. 1b) in order to optimize Van der Waals interactions. This angle depends on the nature of the interfacial bond, the hybridization of the graft atom orbital, the chain length and the substrate. The orientation of dipolar molecules of SAMs formed on a particular surface can be evaluated by using Polarized Modulated Infrared Reflection Absorption Spectroscopy (PM-IRRAS) spectra and IR spectra of the isotopically dispersed molecules in a KBr pellet [22].

The direction of the transition dipolar moments M_i for a vibration i was taken from [13, 23]. Applying the selection rule on a metallic substrate we can write for the PM-IRRAS signal:

$$I(M_i) = k.(M_i.E)^2 = k.M_i^2E^2\cos^2(M_i,E) = k.M_i^2E^2F_i(\alpha,\beta) \qquad (1)$$

, where $\boldsymbol{E}$ is the electric field at the surface, α is the tilt angle, and β is the twist angle, and k a constant. We can express the angles [13] by:

$$\beta = \arctan\sqrt{\frac{I_N A_M}{I_M A_N}} \quad \alpha = \arctan\sqrt{\frac{I_M A_L}{I_L A_M \cos^2\beta}}; \qquad (2)$$

Here I_N, I_M, and I_L are the areas under the curve of the PM-IRRAS spectrum associated with the peaks at 815 cm^{-1} (N), 1601 cm^{-1} (M) and 1517 cm^{-1}(L) for FBPS and 825 cm^{-1} (N), 1086 cm^{-1} (M) and 1475 cm^{-1} (L) for BPS. A_N, A_M and A_L are the areas under the absorbance spectra of the molecules dispersed in a KBr pellet.

2.4. Device fabrication

To determine the effect of SAM treatment on the performance of Cu as the electrode in an electronic device, planar diodes (see Fig. 2 for a simplified sketch) having differently treated (combination of preliminary oxidative treatment and grafting of a bifunctional self-assembled monolayer based on FBPS or BPS) Cu electrodes and DNTT as active material, were constructed; this type of diode structure is generally used in various electronic devices such as OPV, OFET, OLED, etc and was previously described [13] . A 10 nm-thick Al layer was deposited on the glass substrate by using a shadow mask. This adhesion layer of Al was used to improve the adhesion of copper and to avoid its degradation during the chemical treatments that will follow. After that, two 2.5 mm-long and 50 nm-thick Cu electrodes were formed by evaporating Cu through the same mask by vacuum evaporation (10^{-4} Pa). The distance between two electrodes was fixed at 30 μm. After that, the Cu electrodes were treated in different ways and a 50 nm-thick layer of semiconductor (DNTT) was deposited by vacuum evaporation at 10^{-5} Pa.

2.5. Characterization

Static contact angles of different SAMs with water were measured in water-saturated air by a Digidrop (GBX, France) contact angle measurement system. PM-IRRAS

measurements of different samples were performed on an argon-purged Nicolet 860 FTIR spectrometer with a IR beam at a grazing angle of 85°. X-Ray photoelectron spectroscopy (XPS) signals were recorded using a Thermo VG ESCALAB 250 system equipped with a monochromatic Al Kα X-ray source (1486:6eV) and 400 μm-sized X-ray beam, with a magnetic lens, which increases the electron acceptance angle and hence the sensitivity. The spectra were acquired in the constant analyzer energy mode, with a pass energy of 100 and 40 eV for the survey and the narrow regions, respectively. The peak binding energy positions were calibrated by setting the aromatic C1s of SAMs at 284.2eV or the contamination carbon C1s at 285 eV in absence of SAMs. X-Ray diffractions profiles of DNTT films on differently treated Cu surfaces were recorded in air on a Rigaku Ultima IV diffractometer with a Cu Kα source (λ = 1.54187 Å). Current (I)-voltage (V) curve of diodes were recorded on a Keithley 4200 semiconductor system.

3. Results and Discussion

We first measured contact angles of different SAMs with ultra-pure water. These measurements indicate that both BPS and FBPS SAM-grafted oxidized copper substrates are hydrophobic; this corresponds to a low surface free energy, which is compatible with the hydrophobic nature of the terminal groups of these SAMs. For BPS SAM the contact angle was 109° and for FBPS it was 95.7°.These high angles show that the layers are close-packed. To determine the orientation of the SAMs toward the Cu substrate normal, we recorded their PM-IRRAS spectra.

3.1 Formation and orientation of the SAMs on copper substrates

The PM-IRRAS spectra of different SAMs grafted onto Cu were studied under various conditions

3.1.1 Influence of RCA treatment of copper substrate

Since it is very difficult to work with oxide-free copper at atmospheric pressure, we worked on substrates of copper voluntarily oxidized in a reproducible manner. This controlled oxidation was produced by RCA treatment at different ratios (v/v/v) of NH_3:H_2O_2:H_2O. In Fig. 3 the spectrum 'b' and 'c' depicts the PM-IRRAS of FBPS monolayers grafted on (1/1/16000) and (1/1/4000) RCA-treated copper substrate respectively. Clearly, the ratio of the polarized bands at 1600 and 1484 cm^{-1}(L), 1516 cm^{-1}(M) and 813 cm^{-1}(N) are different in the SAMs and in the dispersed molecules (KBr pellet). Notably the M and N polarized bands are smaller in the SAMs. By eqn. 2 we estimate (Table 1) the orientation angles of the molecules: $\alpha = 31° \pm 3$, $\beta = 39° \pm 3$.

RCA treatment of the copper substrate gives a clean but possibly rough copper oxide layer that can diminish the apparent orientation and organization toward the metallic surface. It is necessary to find a compromise between the cleanliness of the substrate and getting relevant values of orientation angles. The best compromise is obtained when the molecular orientation is closest to normal, i.e. when the RCA conditions are around 1/1/16000. From Table 1 it can be seen that the FBPS molecules appear to be less well oriented (tilt angle $\alpha = 35^{o}$) toward the surface normal on the Cu electrode treated with highly concentrated RCA (NH_3:H_2O_2:H_2O = 1:1:4000). Interestingly, the orientation of FBPS molecules on the RCA-treated Cu surface is the best ($\alpha = 31^{o}$) with the RCA ratio of (1:1:16000). At lower concentration (1:1:32000), the angle of inclination increases because the concentration of the oxidizing solution is not sufficient to remove the contamination, which can prevent the molecules from organizing and orienting on the surface. Let us remind that the average tilt angle of a randomly arranged molecule is the magic angle i.e. 54.7° [24].

To compare the orientation of FBPS and BPS on copper electrodes we further recorded PM-IRRAS spectra (Fig. 4) of BPS monolayers adsorbed on RCA-Cu (NH_3:H_2O_2:H_2O = 1:1:16000) surface and the IR spectra of the molecules in a KBr pellet. The twist (β) and tilt (α) angles of BPS molecules absorbed on the RCA-treated Cu surface (Table 2) were calculated by eqn. 2. Here it should be noted that the absorbed BPS molecules are less well oriented ($\alpha = 47^o$) on the RCA-treated Cu surface than FBPS molecules.

On an Au substrate, the difference in the organization of BPS and FBPS SAMs is less (Table 3) and both molecules are oriented. The location of some vibrations depends strongly on the nature and state of the atom bound to the sulfur, i.e. H, Au or Cu/CuO.

Under these conditions the oxide thickness for FBPS and BPS was estimated by grazing incidence X-ray experiments using the interference effect of the copper oxide layer (Fig.9); similar value of the thicknesses were obtained whatever the nature of the thiol or the copper oxide: d_{ox}= 9 ±1nm (1/1/16000 RCA treatment).

3.1.2 Effect of the water in the thiol solution

The copper substrate oxidized by RCA treatment is orange-gold-brown. After dipping in the thiol FBPS solution, the color changes or not depending on the water present in the dichloromethane. In very dry (SD) solvent or freshly distilled CH_2Cl_2, the color turns to pink-pearl. Nevertheless, the color does not change if a small amount of water is added to the solvent. For BPS, the color does not change in freshly distilled CH_2Cl_2. The evolution of the IR spectra and XPS spectra (see section 4.2) with the amount of water was recorded. Fig. 5 shows the PM-IRRAS spectra of FBPS monolayers with increasing amounts of water from (a) to (c). First, the tilt angle decreases when the solvent is carefully dried and increases when water is added (Table 3). This indicates a better FBPS SAM organization with lower amount of water in thiol solution. Secondly, some bands shift with increasing amounts of water, such

as the γCH op from 816 $cm^{-1}$to 808 cm^{-1} (Table 3). The ν(C=C) band around 1600 cm^{-1} is particularly interesting since with increasing water a new band appears at 1592 cm^{-1} as a shoulder of the band at 1604 $cm^{-1}$and become even larger than the latter (Table 3). On Au this band is located at 1605 cm^{-1} and at 1601 cm^{-1} in a KBr pellet (Table 3). This confirms the relationship between the band wave number and the nature of the interfacial bond. Moreover, this suggests that the nature of the bond between the sulfur and the copper oxide is different in Au, Cu/BPS and Cu/FBPS. The nature of copper oxide and its interaction with the thiols was analyzed by XPS.

3.2 Interaction between the FBPS and BPS thiols with copper oxide

To understand the different behaviors of BPS and FBPS and of the effect of water in the solvent, the XPS spectra of different SAMs on Cu were further studied. In Fig. 6 the XPS Cu_{2p} spectrum with RCA treatment is compared to those of FBPS and BPS SAMS adsorbed on the RCA-treated Cu. The XPS spectra of RCA (1:1:16000)-treated Cu surface have distinctive features at binding energies *P1* 932.9 eV, *P2* 934.7 eV, *P3* 940.6-944 eV, *P4* 952.4 eV, *P5* 954.4 eV and *P6* 962.6 eV. These are assigned to cuprous oxide (Cu_2O) and/or Cu (*P1*), cupric oxide (CuO) and hydroxide ($Cu(OH)_2$ (*P2* and *P3*) , Cu_2O (*P4*) , CuO (*P5* and *P6*) [25-27]. We exclude the possibility that the P1 and P4 peaks could be attributed to metallic Cu, since the metal is not significantly observed on the LMM spectrum of the same sample around 919.1 eV (Fig. 7 (spectrum a)). For comparison, Fig. 7 (spectrum b) shows the presence of Cu(0) after the Cu substrate is rinsed and the oxide layer dissolved with citric acid. Then when the Cu substrate is RCA-treated, the outermost oxide layer masks the Cu(0) metal . Let us remark that the depth of analysis is larger in the LMM spectra located at higher kinetic energy. Thus the RCA-Cu surface contains both cupric (CuO) and cuprous (Cu_2O)

oxides. Interestingly, when FBPS SAM is grafted on the RCA-Cu surface, peaks *P2, P3, P5* and *P6* vanish. This implies that all the CuO phases of the RCA-Cu surface have been reduced to Cu_2O during the grafting of FBPS SAM. BPS does not significantly reduce the CuO phase to Cu_2O, and the RCA-Cu surface contains a mixture of CuO and $Cu(OH)_2$ phases and possibly a little Cu_2O.

To determine the implications of these phenomena, we further analyzed the XPS S2p spectra of differently treated Cu surfaces. In Fig. 8a, b and under the same conditions as Fig. 5, the influence of the amount of water in the CH_2Cl_2 is shown in the S2p spectra of FBPS/RCA Cu. The S2p sulfur doublet (2p3/2, 2p1/2) is observed at 162.2 and 163.4 eV with an intensity ratio of 2. With added water, another wide peak at 167eV increases strongly and its intensity goes from 6% to 22% of total sulfur. This peak is characteristic of oxidized sulfur such as sulfinic ($-SO_2H$) or sulfonic species ($-SO_3H$) is observed at ca. 167.7 eV, according to the equation:

$$FBP\text{-}SH + 3H_2O \rightarrow FBP\text{-}SO_3H + 5H^+ + 5e^-$$

In the case of the BPS-grafted RCA-Cu substrate (Fig. 8c), the amount of oxidized sulfur ($-SO_2H$, $-SO_3H$) is larger (39%) with a very broad peak at around 167 eV. Clearly the presence of water promotes, strongly for BPS and just weakly for FBPS, the extensive oxidation of the sulfur to SOx species (S(III) and S(V)). These species remain bonded to the copper surface and may prevent bulk reduction of Cu (II). In the absence of water, the oxidation of the -SH moiety should give only disulfide that might desorb partially in the solution allowing reduction to continue. Careful inspection of the decomposition of the S2p peak around 163eV reveals a second doublet that is only important with the BPS (163.25 eV - 164.42 eV: ratio1.9 and 30% of the total sulfur). This value may indicate the presence of disulfide BP-S-S-BP attached to the oxidized copper.

$$2\ FBP\text{-}SH \rightarrow FBP\text{-}S\text{-}S\text{-}PBF + 2H^+ + 2\ e^-$$

In the case of FBPS (Figures 8a, b) few disulfide molecules remain anchored on the surface with a S2p doublet (163.2 ± 0.1eV 164.3 ± 0.1 eV, ratio 1.8 ± 0.1), which represents 6-12% of the total sulfur.

In conclusion, FBPSH reduces the CuO to Cu_2O with a limited oxidation of sulfur to disulfide. The presence of the fluorine atom, an electron-withdrawer, on the aromatic ring, is expected to moderate the reducing power by stabilizing the initial reagent more than the FBPS• radical produced by the oxidation [28].

BPS molecules oxidize extensively to SOx species, which remain on the surface and may prevent kinetically bulk reduction of the CuO. The presence of these contaminants on the oxidized Cu surface is the main reason behind the disorganization of the BPS molecules. In the same way, the presence of water increases the reducing strength of FBPS and tends to produce attached SOx species.

3.3 Structure of DNTT film on SAM-modified copper substrates

The main objective of this work was to make the Cu metal suitable as an electrode material for a diode by proper surface treatment; therefore, we further evaporated an organic semiconductor (OSC), DNTT, onto both BPS and FBPS grafted on the RCA-Cu substrate and recorded their out-of-plane XRD profiles. It is observed (Fig. 9) that the DNTT layer deposited onto a BPS SAM grafted onto RCA-oxidized Cu is amorphous whereas the out-of-plane XRD profile of the DNTT layer formed onto FBPS SAM/Cu_2O shows a distinct peak around $2\theta = 5.39^{o}$ associated with the (001) plane of the DNTT film [29]. This confirms the formation of a moderately crystallized DNTT layer on this SAM. The estimated interlayer spacing from the (001) plane is 1.64 nm. To complete these results we further recorded PM-IRRAS spectra (Fig. 10) of the DNTT layer formed on the two SAMs grafted onto RCA-Cu

and the spectrum of the SC in a KBr pellet. The values of the twist and tilt angles of DNTT molecules on the SAMS are reported in Table 4. The DNTT molecules are poorly oriented (tilt angle α' = 50°) on the BPS SAM grafted on oxidized Cu whereas the DNTT molecules deposited onto the FBPS/Cu_2O are well oriented towards the surface normal (α' = 24°). Thus, the DNTT layer organization reflects that of the SAM molecules: a good assembly of the surface on which the DNTT grows ensures the crystallization of the deposited film. On Au substrate, the DNTT film crystallization and molecular orientation are very similar for BPS and FBPS SAMs (not shown), which are both, oriented in this case (Table 4). In contrast to the copper substrate, both the BPS and the FPS SAMs are well oriented and induce the SC organization.

3.4 Electrical properties of diodes with SAM-treated copper substrates

Fig. 11 represents the characteristic current (I) - voltage (V) curve of a diode formed by DNTT/Cu with FBPS SAM grafted onto RCA-oxidized Cu and Au used as electrode. The diode formed with a bare oxidized Cu electrode and BPS SAM grafted on the oxidized Cu electrode does not function properly. Therefore, we are unable to show any current (I) – voltage (V) curves for these two diode structures. The I-V curve follows space-charge-limited current (SCLC) behavior. The slope of the curve is around 1 in the log-log plot at low voltages and gradually passes to a slope of almost exactly 2 at higher voltages (threshold voltage, V_{th} = 24.72 V). The variation of current (I) with applied voltage for this type of diode structure is well described by eqn. 3 [30-31], since we are dealing here with a coplanar geometry with a film of thickness h much lower than the channel length L.

$$\frac{I}{W} = \frac{2}{\pi} \varepsilon \mu \frac{V^2}{L^2} \qquad (3)$$

where, ‘W’ is the channel width, ‘μ’ is the bulk effective mobility of the semiconductor, and ‘ε’ is the dielectric constant of the semiconductor. By analyzing the (I) = f(V) curve of the diode with the help of eqn. 3, the bulk mobility (at space charge region) of DNTT deposited onto FBPS SAM grafted on oxidized Cu electrode was estimated. The value is ~ 0.35 $cm^2.V^{-1}.s^{-1}$ for the Cu_2O electrode and ~1.8 $cm^2.V^{-1}.s^{-1}$ for an Au electrode. Here, well-organized FBPS molecules of the SAM help to deposit a crystalline DNTT layer. With the support of the results obtained with BPS adsorbed on gold electrodes [13], we can conclude that the organizations of both the SAMs and the SC layer are insufficient to observe a good effective mobility of the SC: the dipole formed by highly oriented molecules -such as FBPS -between the metal and semiconductor is required to reduce the hole energy barrier between the electrode and the semiconductor. Due to these two positive effects, the DNTT semiconductor-based diode with FBPS grafted on an oxidized (by RCA (1/1/16000)) Cu electrode operates properly even if the effective mobility of the DNTT film is less than for gold. On the other hand, a layer of DNTT deposited on the BPS SAM / CuO / Cu is amorphous and the modified copper electrode is unable to inject the carriers unlike the Au electrode.

4. Conclusion

We have tested the utility of SAMs of two different conjugated molecules, BPS and FBPS, grafted on a Cu substrate, as possible replacements for gold electrodes in electronic devices. This goal was achieved with a mobility of 0.35 $cm^2.V^{-1}.s^{-1}$ for FBPS/DNTT. The conditions are: i) the starting Cu electrode is cleaned/oxidized and covered by a thin CuO layer; ii) the reduction of CuO to Cu_2O by FBPS which oxidizes only to disulfide $(FBPS)_2$; iii) the formation of an oriented and dipolar SAM on the Cu_2O substrate thanks to limited thiol oxidation and, consequently, iv) both the diminution of the hole injection barrier due to the

oriented dipole and the presence of a crystalline, oriented DNTT film. For BPS SAMs, the thiol is extensively oxidized and this generates -SOx species that limit the organization in the SAM and hinder DNTT organization.

ACKNOWLEDGMENTS

Korea Electric Power Corporation supported our research (Grant number: R19XO01-05). The National Research Foundation of Korea (NRF-2019K1A3A1A21031246) also supported our research. We thank Florian Gregoire and Meriem Bouriga for their help with chemical experiments, Jean-Charles Vanel and Yvan Bonnassieux (LPICM école Polytechnique) for their support in electrical measurements, and Dr John S. Lomas was editing the text of the paper.

References

[1] H.-W. Chen, J.-H. Lee, B.-Y. Lin, S. Chen, S.-T. Wu, Liquid crystal display and organic light-emitting diode display: present status and future perspectives, Light: Science & Applications, 7 (2018) 17168-17168.

[2] J. Sheng, K.-L. Han, T. Hong, W.-H. Choi, J.-S. Park, Review of recent progresses on flexible oxide semiconductor thin film transistors based on atomic layer deposition processes, Journal of Semiconductors, 39 (2018) 011008.

[3] S. Biswas, H. Kim, Solar Cells for Indoor Applications: Progress and Development, Polymers, 12 (2020) 1338.

[4] S. Biswas, Y.-J. You, J. Kim, S.R. Ha, H. Choi, S.-H. Kwon, K.-K. Kim, J.W. Shim, H. Kim, Decent efficiency improvement of organic photovoltaic cell with low acidic hole transport material by controlling doping concentration, Applied Surface Science, 512 (2020) 145700.

[5] R. Pode, Organic light emitting diode devices: An energy efficient solid state lighting for applications, Renewable and Sustainable Energy Reviews, 133 (2020) 110043.

[6] Y. Wu, Y. Li, B.S. Ong, P. Liu, S. Gardner, B. Chiang, High□performance organic thin□film transistors with solution□printed gold contacts, Advanced Materials, 17 (2005) 184-187.

[7] J.-P. Hong, A.-Y. Park, S. Lee, J. Kang, N. Shin, D.Y. Yoon, Tuning of Ag work functions by self-assembled monolayers of aromatic thiols for an efficient hole injection for solution processed triisopropylsilylethynyl pentacene organic thin film transistors, Applied Physics Letters, 92 (2008) 131.

[8] N. Zhang, Y. Hu, X. Liu, Transparent organic thin film transistors with WO3/Ag/WO3 source-drain electrodes fabricated by thermal evaporation, Applied Physics Letters, 103 (2013) 120_121.

[9] I. Campbell, S. Rubin, T. Zawodzinski, J. Kress, R. Martin, D. Smith, N. Barashkov, J. Ferraris, Controlling Schottky energy barriers in organic electronic devices using self-assembled monolayers, Physical Review B, 54 (1996) R14321.

[10] B. Choi, J. Rhee, H.H. Lee, Tailoring of self-assembled monolayer for polymer light-emitting diodes, Applied Physics Letters, 79 (2001) 2109-2111.

[11] B. de Boer, A. Hadipour, M.M. Mandoc, T. van Woudenbergh, P.W. Blom, Tuning of metal work functions with self□assembled monolayers, Advanced Materials, 17 (2005) 621-625.

[12] Y. Vaynzof, T.J. Dennes, J. Schwartz, A. Kahn, Enhancement of electron injection into a light-emitting polymer from an aluminum oxide cathode modified by a self-assembled monolayer, Applied Physics Letters, 93 (2008) 328.

[13] H. Kim, Z. Meihui, N. Battaglini, P. Lang, G. Horowitz, Large enhancement of hole injection in pentacene by modification of gold with conjugated self-assembled monolayers, Organic electronics, 14 (2013) 2108-2113.

[14] G. Heimel, L. Romaner, E. Zojer, J.-L. Brédas, Toward control of the metal− organic interfacial electronic structure in molecular electronics: A first-principles study on self-assembled monolayers of π-conjugated molecules on noble metals, Nano letters, 7 (2007) 932-940.

[15] S. Khodabakhsh, B.M. Sanderson, J. Nelson, T.S. Jones, Using Self-Assembling Dipole Molecules to Improve Charge Collection in Molecular Solar Cells, Advanced Functional Materials, 16 (2006) 95-100.

[16] Z. Jia, V.W. Lee, I. Kymissis, L. Floreano, A. Verdini, A. Cossaro, A. Morgante, In situ study of pentacene interaction with archetypal hybrid contacts: Fluorinated versus alkane thiols on gold, Physical Review B, 82 (2010) 125457.

[17] G. Kikugawa, T. Ohara, T. Kawaguchi, I. Kinefuchi, Y. Matsumoto, A molecular dynamics study on heat conduction characteristics inside the alkanethiolate SAM and alkane liquid, International Journal of Heat and Mass Transfer, 78 (2014) 630-635.

[18] D.T. Valley, M. Onstott, S. Malyk, A.V. Benderskii, Steric hindrance of photoswitching in self-assembled monolayers of azobenzene and alkane thiols, Langmuir, 29 (2013) 11623-11631.

19) P. Marmont, N.Battaglini, P. Lang, G. Horowitz, J. Hwang, A. Kahn, C. Amato, P. Calas, Improving charge injection in organic thin-film transistors with thiol-based self-assembled monolayers Organics Electronics 9 (2008) 419.

[20] M.S. Inkpen, Z.F. Liu, H. Li, L.M. Campos, J.B. Neaton, L. Venkataraman, Non-chemisorbed gold–sulfur binding prevails in self-assembled monolayers, Nature chemistry, 11 (2019) 351-358.

[21] K. Hong, J.W. Lee, S.Y. Yang, K. Shin, H. Jeon, S.H. Kim, C. Yang, C.E. Park, Lower hole-injection barrier between pentacene and a 1-hexadecanethiol-modified gold substrate with a lowered work function, Organic electronics, 9 (2008) 21-29.

[22] P. Lang, G. Horowitz, P. Valat, F. Garnier, J. Wittmann, B. Lotz, Spectroscopic evidence for a substrate dependent orientation of sexithiophene thin films deposited onto oriented PTFE, The Journal of Physical Chemistry B, 101 (1997) 8204-8211.

[23] J.F. Kang, A. Ulman, S. Liao, R. Jordan, G. Yang, G.-y. Liu, Self-assembled rigid monolayers of 4 ‘-substituted-4-mercaptobiphenyls on gold and silver surfaces, Langmuir, 17 (2001) 95-106.

[24] Simpson G.J., Rowlen K.L. An SHG Magic Angle: Dependence of Second Harmonic Generation Orientation Measurements on the Width of the Orientation Distribution, J. Am. Chem. Soc. , 121 (11), (1999) 2635–2636.

[25] M.C. Biesinger, B.P. Payne, A.P. Grosvenor, L.W. Lau, A.R. Gerson, R.S.C. Smart, Resolving surface chemical states in XPS analysis of first row transition metals, oxides and hydroxides: Cr, , Mn, Fe, Co and Ni, Applied Surface Science, 257 (2011) 2717-2730.

[26] M.C. Biesinger, Advanced analysis of Copper X-ray photoelectron spectra; Surf.Interface Anal ., 49(2017) 1325-1334

[27] Zheng, J. Y., Van, T. K., Pawar, A. U., Kim, C. W., & Kang, Y. S. One-step transformation of Cu to Cu2O in alkaline solution. RSC Advances, 4(36), (2014) 18616-18620.

[28] J. L. Garcıa Ruano, A. Parra and J. Aleman Efficient synthesis of disulfides by air oxidation of thiols under sonication, *Green Chem.*, 2008, 10, 706–711

[29] T. Yamamoto, K. Takimiya, Facile Synthesis of Highly π-Extended Heteroarenes, Dinaphtho[2,3-b:2‘,3‘-f]chalcogenopheno[3,2-b]chalcogenophenes, and Their Application to Field-Effect Transistors, J. Am. Chem. Soc. 129, 8,(2007) 2224–2225.

[30] J. Geurst, Theory of space□charge□limited currents in thin semiconductor layers, physica status solidi (b), 15 (1966) 107-118.

[31] P. Knoll, R. Zuleeg, Space-charge-limited currents in heteroepitaxial films of silicon grown on sapphire, (1967).

Tables

FBPS / substrate	$\nu_{C=C}$ (cm^{-1}) (M)	γ_{C-Hop} (cm^{-1}) (N)	orientation angles α ± 3°	β ± 5°
FBPS / Au *	1605	818	**32**	38
FBPS / Cu RCA 1/1/4000	1604 1593 sh	816	**35**	48
FBPS / Cu RCA 1/1/16000	1604 1593 sh	813	**31**	39
FBPSH in KBr	1601 sh 1595	813		

Table 1: Wavelengths of some characteristic vibrations and orientation angles of FBPS adsorbed on Au [13] on RCA-treated Cu and in KBr pellet.

	$\nu_{C=C}$ (cm^{-1}) (M)	$\nu_{C=C}$ (cm^{-1}) (L)	ring C-C δ C-H **(M)**	γ_{C-Hop} (cm^{-1}) (N)	orientation angles α ± 3°	β ± 5°
BPS / Cu RCA 1/1/16000	1600 1583	1475	1086	825	**47**	33
BPS/Au	1605	1473	1105	822	34	35
BPSH in KBr	1595	1479	1103.5	826		

Table 2: Wavelength (cm^{-1}) of characteristic vibrations and orientation angles of BPS adsorbed on RCA (1/1/16000)-treated Cu, on Au and in KBr pellet.

water amount in FBPS/ CH_2Cl_2	$\nu_{C=C}$ (cm^{-1}) (M)	γ_{C-Hop} (cm^{-1}) (N)	orientation angles α ± 3°	β ± 5°
low (SD solvent)	1604.7	816	28	38
intermediate (as distilled)	1604 1593 sh	813	31	39
added water 0.05M	1604 sh1593	808	39	55

Table 3: Effect of solvent water on wavelengths (of some characteristic vibrations and on the orientation angles of FBPS adsorbed on RCA-treated Cu.

	DNTT/FBPS /Au	DNTT/BPS/Au	DNTT/FBPS /Cu RCA(1/1/16000)	DNTT/BPS /Cu RCA(1/1/16000)
α' (^{o}) ± 3	21	18	24	50
β' (^{o}) ± 3	40	43	44	51
μ ($cm^2.V^{-1}.s^{-1}$)	1.8	-	0.35	-

Table 4: Tilt and twist angles of the DNTT layer on BPS and FBPS-grafted oxidized Cu substrate

Figures

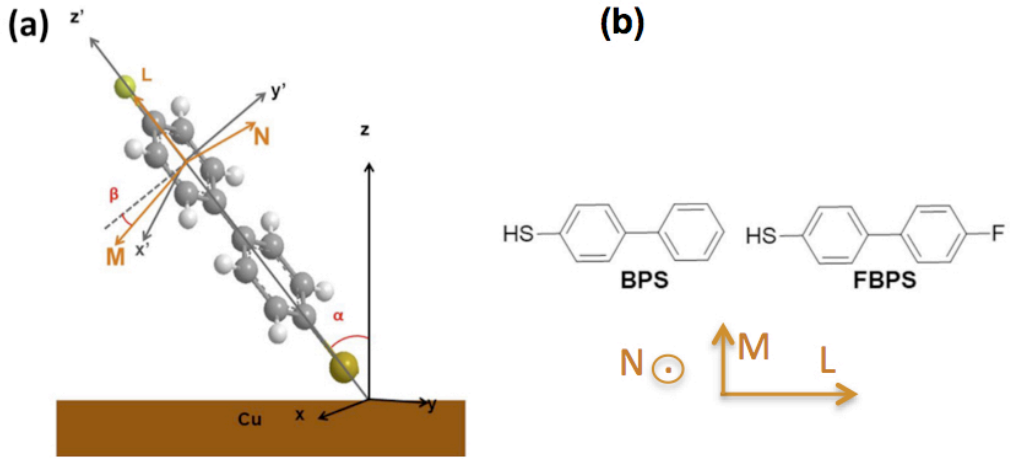

Fig. 1: (a) Orientation of transition dipolar moment associated with the three possible directions of vibration polarization of FBPS; (b) Chemical structures of BPS and of FBPS.

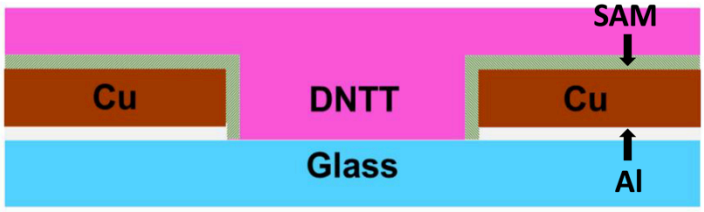

Fig. 2: Schematic and simplified diagram of diode formed by DNTT.

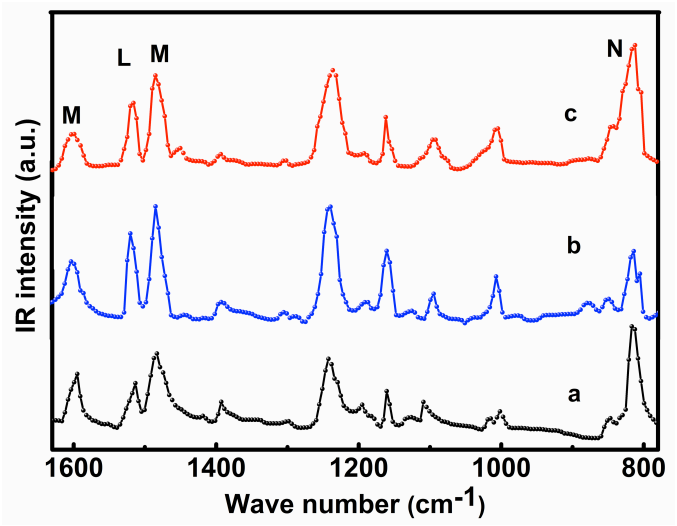

Fig. 3: IR spectrum of FBPS in KBr pellet (a) and effect of Cu treatment by RCA on the PM-IRRAS spectra of FPBS monolayers: b: RCA 1/1/16000; c: RCA 1/1/14000 (see text).

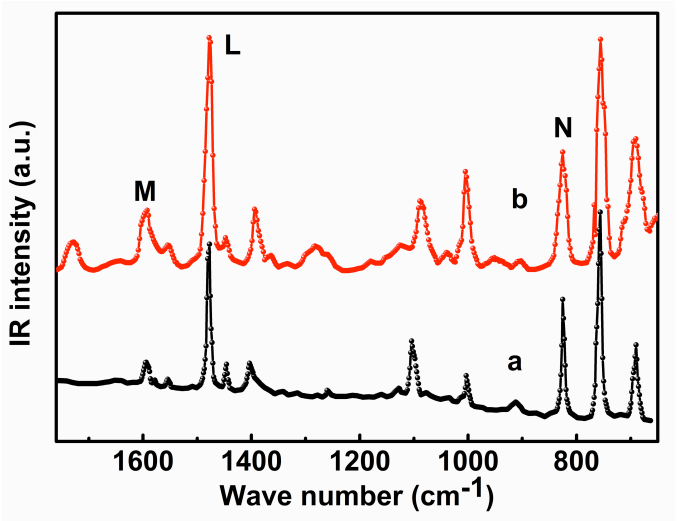

Fig. 4: PM-IRRAS spectra of BPS monolayers adsorbed on RCA (1/1/16000)-treated Cu substrate (b), and BPS molecules in a KBr pellet (a).

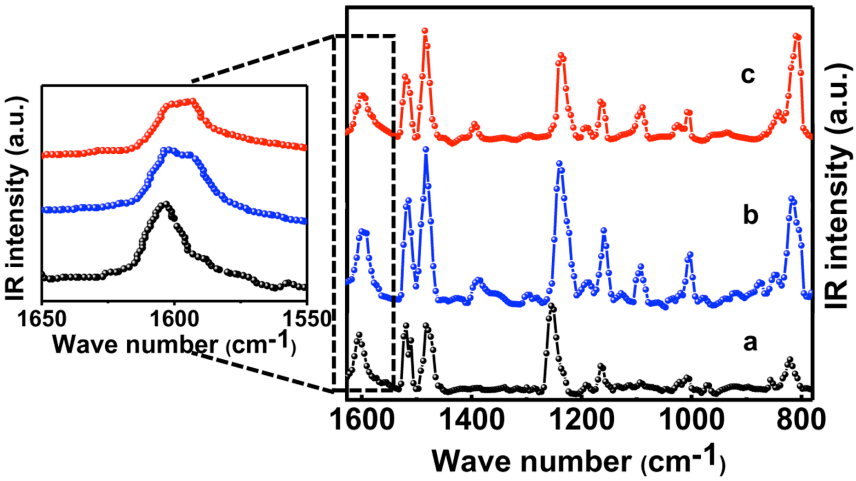

Fig. 5: PM-IRRAS spectra of FPBS monolayers adsorbed at various concentrations of water in CH_2Cl_2 on RCA-treated Cu substrates: a: super-dried; b: after distillation; c: $[H_2O]$ = 0.05M.

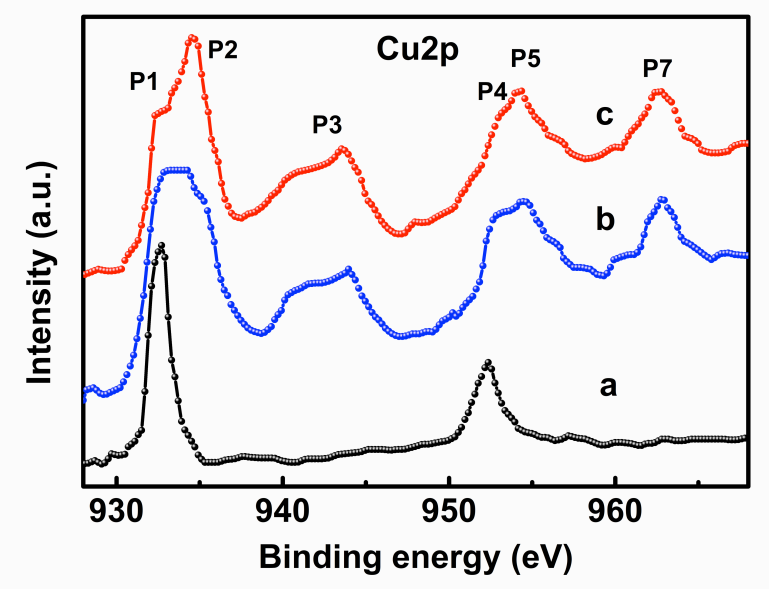

Fig. 6: XPS Cu2p spectra at different Cu treatment conditions: (a) Cu/RCA (1/1/16000)/FBPS; (b) Cu/RCA (1/1/16000); (c) Cu/RCA (1/1/16000)/BPS.

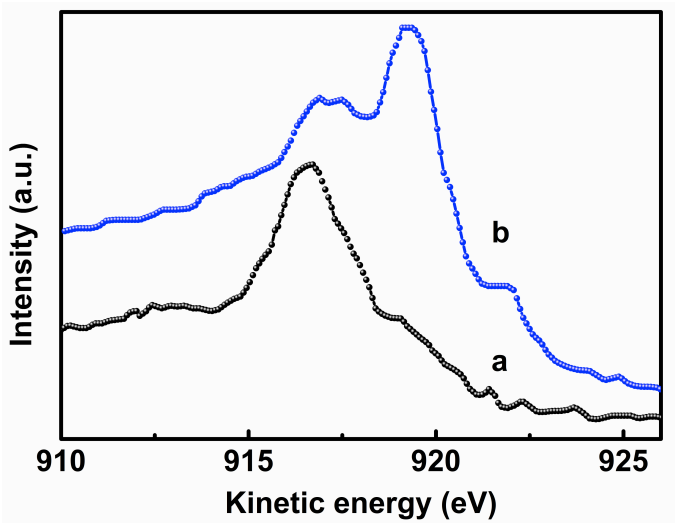

Fig. 7: Cu L3M4, 5M4, 5 spectra of (a) Cu/RCA (1/1/16000)/FBPS; b) FBPS adsorbed on Cu treated by RCA solution and then by citric acid.

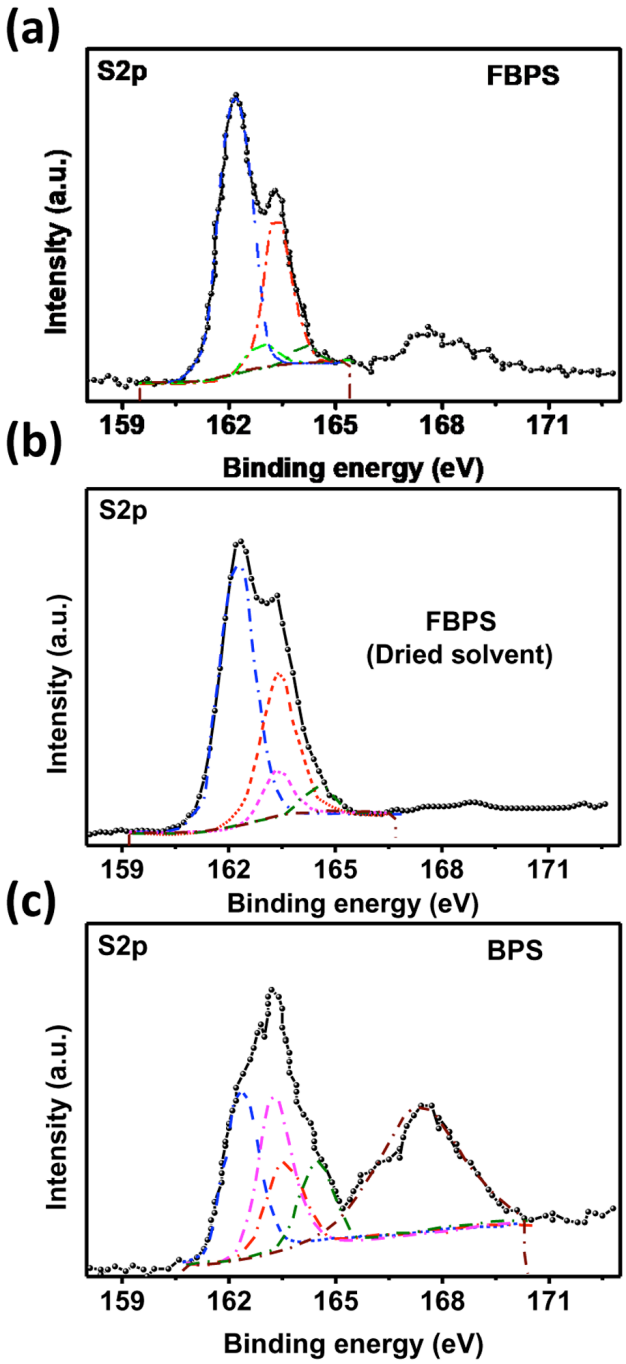

Fig. 8: S2p XPS spectra of (a) FBPS adsorbed on RCA (1/1/16000)-treated Cu, (b) FBPS adsorbed on RCA (1/1/16000)-treated Cu (after the solvent has been carefully dried (SD)), (c) BPS adsorbed on RCA (1/1/16000)-treated Cu.

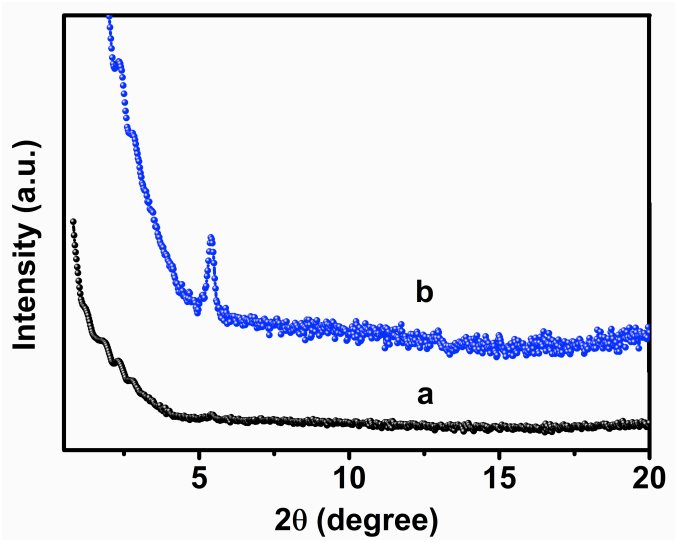

Fig. 9: Out-of-plane XRD spectra of DNTT film formed on (a) BPS- and (b) FBPS- treated Cu substrate.

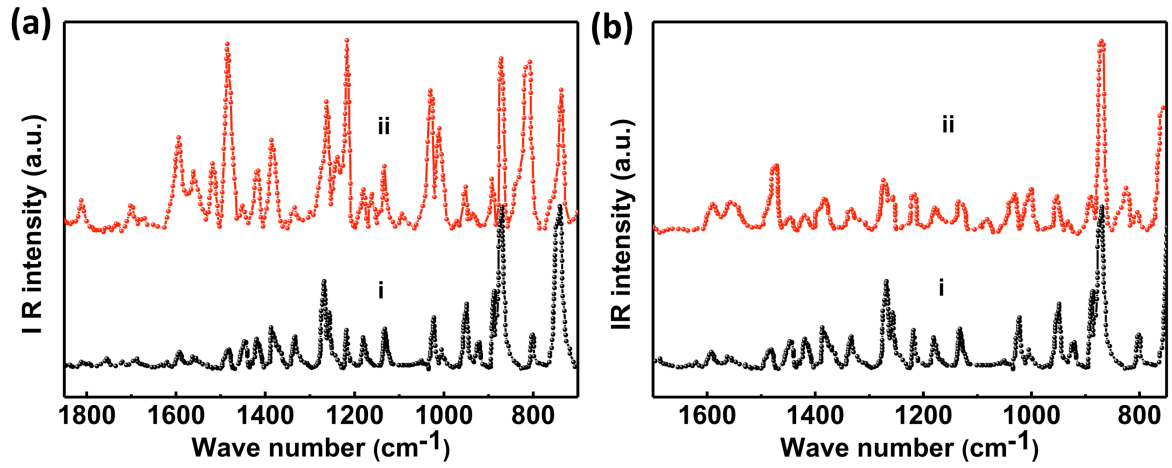

Fig. 10: (a) PM-IRRAS spectra of DNTT layer formed on FBPS-grafted oxidized (by RCA (1/1/16000)) KBr pellet (i) and Cu surface (ii); (b) PM-IRRAS spectra of DNTT layer formed on BPS-grafted oxidized (by RCA (1/1/16000)) KBr pellet (i) and Cu surface (ii).

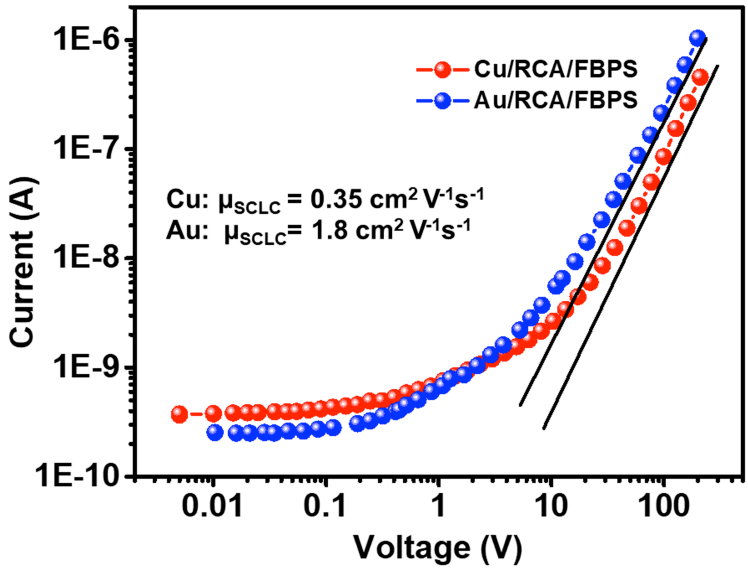

Fig. 11: Characteristic current (I)-voltage (V) curve of the FPBS /DNTT-based diode for both Cu and Au electrode (the lines of best fit have both a slope of 2 (in log-log plot)).